

—Original Paper—

Detection of Late Pleistocene tephtras and cryptotephtras using major element chemistry of glass shards from Chikyu C9001C cores, NW Pacific Ocean

Tabito Matsu'ura^{1*} and Junko Komatsubara²

We reinvestigated tephra and cryptotephra stratigraphy of the Late Pleistocene deep-sea C9001C cores collected during the D/V *Chikyu* shakedown cruise. We identified 26 glass shard concentration horizons (spikes) corresponding to four previously reported tephtras (G1, G2, G3, and G4 from top to bottom). We newly found three visible tephtras and 19 nonvisible cryptotephtras (G0.0–0.9, G1.1–1.4, G2.1–2.5, and G3.1–3.3). We newly correlated spike G0.2 with the Towada-Hachinohe (To-H: MIS 1/2, 15 ka), G0.5 with the Towada-Biscuit 2 (To-BP2: MIS 2, 18 ka), G1.1 with the Komagatake-i (39 ka), G1.2 with the Kutcharo-Shoro (MIS 3, 40 ka), and G3.3 with the Sambe-Kisuki (MIS 5c, 100 ka) tephtras. Spikes G2.2, G2.3, and G2.4 may correlate with the Towada tephtra series (seven correlative candidates), spike G3.1 with an Ontake volcano tephtra (MIS 5b–5c), and spike G3.2 with the Towada-Castera or Towada-Aosuji (both MIS 5b–5d) tephtra. We classified spike G0.1 as reworked materials of the underlying spike G0.2 (To-H), and the combinations of spikes G0.3 and G0.4 and of G0.8 and G0.9 as the result of repeated reworking of the underlying spikes G0.5 (To-BP2) and G1 (To-Of), respectively. We also classified spikes G1.3 and G1.4 as reworked mixtures of Shikotsu-1 tephtra with glass shards from other tephtras. The upward decrease of the glass shard populations above spikes G3 and G4 is interpreted as indicating immediate reworking of the tephtras after initial emplacement. Whether or not a marine tephtra is preserved depends on depositional and post-depositional processes and not simply on the eruptive volume or the distance from source. Nevertheless, cryptotephtras recognized by glass shard concentration horizons in marine cores can provide additional datum planes and contribute to marine tephrostratigraphy.

Keywords : marine tephtra, cryptotephtra, chemical analysis, Chikyu C9001C cores, Late Pleistocene

Received 27 March 2017 ; Revised 24 July 2017 ; Accepted 1 August 2017

- 1 Regulatory Standard and Research Department, Secretariat of Nuclear Regulation Authority (S/NRA/R)
- 2 Geological Survey of Japan, National Institute of Advanced Industrial Science and Technology (AIST)

*Corresponding author:

Tabito Matsu'ura

Regulatory Standard and Research Department, Secretariat of Nuclear Regulation Authority (S/NRA/R)

1-9-9 Roppongi, Minato-ku, Tokyo 106-8450, Japan

tabito_matsuura@nsr.go.jp

Copyright by Japan Agency for Marine-Earth Science and Technology

1. Introduction

Marine tephrostratigraphy has been used for accurate stratigraphic correlation because marine (deep-sea) sediments are long-term and high-time-resolution archives that also contain magnetostratigraphic, microbiostratigraphic and marine oxygen isotopic records (e.g., Buhring and Sarnthein, 2000; Song et al., 2000; Aoki, 2008; Brendryen et al., 2010; Abbott et al., 2011; Davies et al., 2010; Matsu'ura et al., 2014). Tephra layers in deep-sea cores have been recorded in the visual core descriptions (VCDs) made by shipboard scientific parties of ocean drilling programs such as the International Ocean Discovery Program (IODP; before October 2013, the Integrated Ocean Drilling Program), the Ocean Drilling Program (ODP), and the Deep Sea Drilling Program (DSDP). However, tephra layers and tephra-related descriptions in VCDs are sometimes over-recorded, resulting in false positives, or under-recorded (false negatives), giving rise to uncertainties in the tephrostratigraphy due to differences in expedition scope and shipboard conditions (Mahony et al., 2014). Further, even if tephra layers reported in the VCD have been ground-truthed by detailed examination of the core sediments after the expedition, some tephra layers are likely to remain undetected. For example, at ODP Site 1123 at least five overlapping cores were required to recover >99% of all tephras (Allan et al., 2008). At most sites fewer than five cores have usually been retrieved. Particularly when such full coring was not possible, overlooked tephras by VCDs is a significant problem. Therefore, a method for detecting overlooked tephras in deep-sea cores is essential.

To detect nonvisible tephras for establishing a better tephrostratigraphy in existing deep-sea cores, whole sections of each core should be examined for cryptotephras (concentration horizons of tephra-derived grains that do not form visible layers in the sediments) (e.g., Matsu'ura et al., 2014, 2017). In deep-sea sediments, cryptotephras, which are usually recognized as glass shard concentrations, can potentially provide many tephra horizons in addition to the visible tephras (Lowe, 2011, 2014). However, glass shard concentrations can result from not only tephra falls but also redeposition, including reworking and bioturbation of previously deposited tephras (Allan et al., 2008; Griggs et al., 2014; Hopkins et al., 2015). Thus, it is important to discriminate *in situ* tephras from reworked tephras.

In this study, we focused on glass shard

concentration horizons in the Late Pleistocene deep-sea sediments that can be compared with the well-established terrestrial tephrostratigraphy in northeastern Japan. We documented the presence of possible tephras and cryptotephras by counting number of glass shards in the deep-sea samples from the C9001C cores, obtained from the continental slope off Shimokita Peninsula, northeastern Japan, by D/V *Chikyu* during its 2006 shakedown cruise for IODP. We also sampled some terrestrial tephras for comparison. We then correlated the marine tephras with the terrestrial tephras on the basis of the glass shard chemistry. Next, we examined the core lithology at each tephra and cryptotephra horizon and refined the tephra descriptions in the VCD. Further, we interpreted redeposition processes in the marine environment on the basis of vertical glass-shard content and chemistry. Finally, we used these results to refine the tephrostratigraphy of the cores.

2. Regional setting of the study area and description of the Late Pleistocene tephras in C9001C cores

The drilling site of the C9001C cores is on the continental slope off northern Honshu at 1180 m water depth (41.177300°N, 142.201350°E; Aoike, 2007; Fig. 1b). The site is on the non-volcanic forearc about 95 km from the nearest Quaternary volcano (Osore volcano) on the Shimokita Peninsula. However, many other volcanoes lie upwind in the westerlies wind belt, and the site has received tephras from both nearby and distant volcanoes during the Quaternary.

The C9001C cores contain a continuous, 365-m-long marine sequence dated entirely in the Brunhes normal polarity epoch (Kobayashi et al., 2009; Aoike et al., 2010). The cores are subdivided into 40 segments, numbered from 40H to 1H in ascending order, and the boundary between the Middle and the Late Pleistocene (MISs 6 and 5) is at 69.97 mbsf in the 8H core segment. The sediment also includes fallout tephras. Layers of fine ash represent products of distant volcanoes, whereas layers of coarse pumice are more likely to be derived from nearby volcanoes in Honshu or Hokkaido (Fig. 1b). The visible Late Pleistocene tephras at 30.30–30.39 mbsf and at 54.35–54.38 mbsf in the cores have been correlated with the Shikotsu-1 (Spfa-1) and Aso-4 tephras, respectively (Aoike et al.,

2010); a tephra at 52.8 mbsf (just above Aso-4) may be the Kuttara 6 or Kuttara 7 tephra (Kt-6 or Kt-7) (Aoki et al., 2012), and the tephtras at 19.6, 24.8, 25.5, and 61.4 mbsf have been suggested to correlate with the Towada-Ofudo (To-Of), Towada-Godo (To-GP), Komagatake-i (Ko-i), and Toya tephtras, respectively (Hasegawa et al., 2014) (Table 1). Hasegawa et al. (2014) also reported that the horizon that they identified as the To-Of tephra corresponds to MIS 2,

which is younger than the reported age of the tephra (MIS 3: Machida and Arai, 2003). In contrast, Matsu'ura et al. (2014) correlated the To-Of tephra with the tephra horizon at 24.56–24.65 mbsf, which corresponds to MIS 3 and thus matches the reported age of the tephra. Further, Matsu'ura et al. (2014) did not find To-GP in the cores.

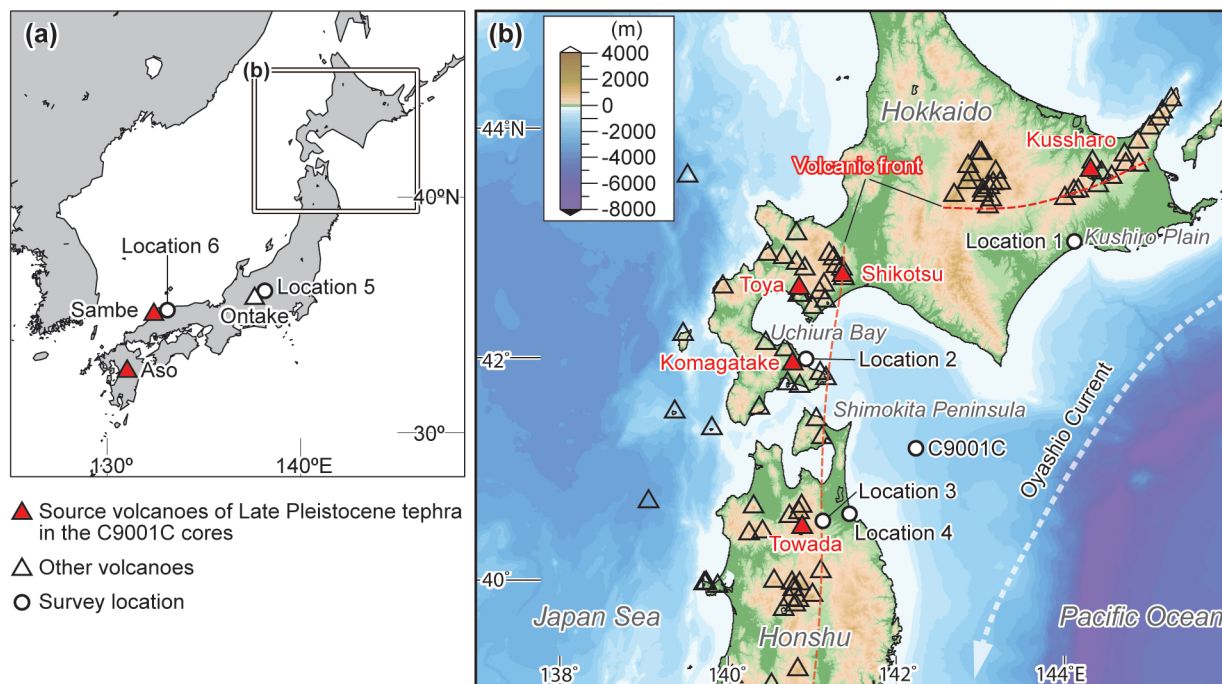


Fig. 1. Map showing locations of volcanoes and ocean drilling sites as well as terrestrial tephra sampling locations (a) in and around Japan and (b) near the C9001C site.

Table 1. Reported tephtras within the C9001C cores.

Visible tephra stratigraphy			Glass shard spike
Aoike (2007)	Aoki et al. (2012)	Hasegawa et al. (2014)	Matsu'ura et al. (2014)*
		To-Of	
		To-GP	To-Of
		Ko-i	
Spfa-1	Spfa-1	Spfa-1	Spfa-1
	Kuttara 6 or 7		
Aso-4	Aso-4	Aso-4	Aso-4
		Toya	Toya

*Using criterion of >1500 glass shards per 3000 grains for tephra detection.

3. Materials and methods

We used core samples from the archived halves of sections 1H (MIS 1) to mid 8H (MIS 6/5) of the C9001C cores that were originally collected and reported by Matsu'ura et al. (2014) (Fig. 2). We also collected outcrop samples of the terrestrial tephtras To-H, To-BP2, To-Of, Ko-i, Kutcharo-Shoro, Ontake-Pumice 1, and Sambe-Kisuki from loess deposits (locations 1–6; Fig. 1b). All samples were sieved under running water through disposable 0.125-mm and 0.0625-mm sieves that were changed between samples to prevent any contamination. The residues were dried, embedded in resin, and mounted on slides. We determined the grain assemblage under the microscope in polarized light with point counters.

To distinguish tephtras and cryptotephtras, we applied a criterion of more than 300 glass shards per 3000 grains to identify high-concentration horizons of volcanogenic materials (hereafter referred to as spikes). Our intention was to detect more spikes than we did previously using the criterion of more than 1500 glass shards per 3000 grains (Matsu'ura et al., 2014). We then handpicked glass shards from each spike for chemical analyses by selecting and polishing 10–15 glass shards from each. The major element compositions were analyzed by using an energy-dispersive electron probe X-ray microanalysis (EPMA) system (Horiba Emax Energy EX-250 or Horiba Emax Evolution EX-270) at Furusawa Geological Survey. Major elements were measured by scanning a 4- μm square area of the targeted grain with a counting time of 150 s (EX-250) or 50 s (EX270), an accelerating voltage of 15 kV, and a beam current of 0.3 nA. Different counting times were used with the two EPMA systems because the sensitivity of the detector differed. The ZAF procedure was applied to correct for atomic number, absorption, and fluorescence effects.

Measurement data obtained by the EPMA systems were calibrated against primary reference materials (synthetic oxide crystals with contents >99.99% of each of SiO_2 , Al_2O_3 , TiO_2 , MnO , and MgO , and monocrystals with contents >99.99% of NaCl , KCl , and CaF_2 , provided by the Nakazumi Crystal Laboratory) and also checked against measurements of secondary standard glasses, namely, MPI-DING reference glasses provided by the Max Planck Institut fuer Chemie (Jochum et al., 2006; Kuehn et al., 2011).

4. Stratigraphy and chemistry of glass shards in spikes

Glass shards at concentrations of more than 1500 shards per 3000 grains in the Late Pleistocene sediments formed four spikes, which were given the integer numbers G1–G4 (Matsu'ura et al., 2014: Table 1; Figs. 2 and 3). Shards at concentrations of more than 300 per 3000 sediment grains formed an additional 22 spikes (G0.0–G0.9, G1.1–G1.4, G2.1–G2.5, and G3.1–3.3). Major element compositions of the glass shards are shown in Fig. 4 by spikes.

Spike G0.0 (9.56–9.66 mbsf, MIS 1) included 336 shards. It corresponds to a “silt-bearing ash” described as 1 cm thick in the VCD (Aoike, 2007), and we also observed a very fine sand-sized ash layer at 9.56–9.57 mbsf (Fig. 3). Most of the shards in this spike had a wide range of SiO_2 and low K_2O (75.9–79.2 and 1.3–1.8 wt.%, respectively), and some had broad SiO_2 and K_2O ranges (76.7–78.4 and 2.6–5.0 wt.%, respectively).

Spike G0.1 (9.86–10.06 mbsf, MIS 1) included 412–440 shards. It corresponds to “silty clay” in the VCD (Aoike, 2007). We observed scattered sand grains in this horizon (Fig. 3), but we did not find any indication of an ash layer. Most of the shards had a wide SiO_2 range (72.3–78.1 wt.%) with low K_2O (1.2–1.8 wt.%), and some had broad SiO_2 and K_2O ranges (73.2–78.1 and 2.5–5.2 wt.%, respectively).

Spike G0.2 (10.46–10.66 mbsf, MIS 1) included 314–828 shards. It corresponds to “silty clay” with an accessory description of “sand scattering” in the VCD (Aoike, 2007). We confirmed this description by our core examination (Fig. 3), but we found no other indication of an ash layer. Shards had wide-ranging SiO_2 (72.9–78.0 wt.%) and low K_2O (1.1–1.4 wt.%), but one shard had high SiO_2 and moderate K_2O (74.9 and 2.0 wt.%, respectively).

Spike G0.3 (12.27–12.37 mbsf, MIS 2) included 320 shards. It corresponds to “silty clay” in the VCD (Aoike, 2007) with no indication of an ash layer. We confirmed this description by our core examination (Fig. 3). Five shards had a wide range of SiO_2 (75.3–77.4 wt.%) and low K_2O (1.3–1.4 wt.%). One shard had high SiO_2 and very low K_2O (77.4 and 0.7 wt.%, respectively), and nine shards had broad ranges of SiO_2 and K_2O (70.9–77.8 and 3.0–5.3 wt.%, respectively).

Spike G0.4 (12.47–12.67 mbsf, MIS 2) included

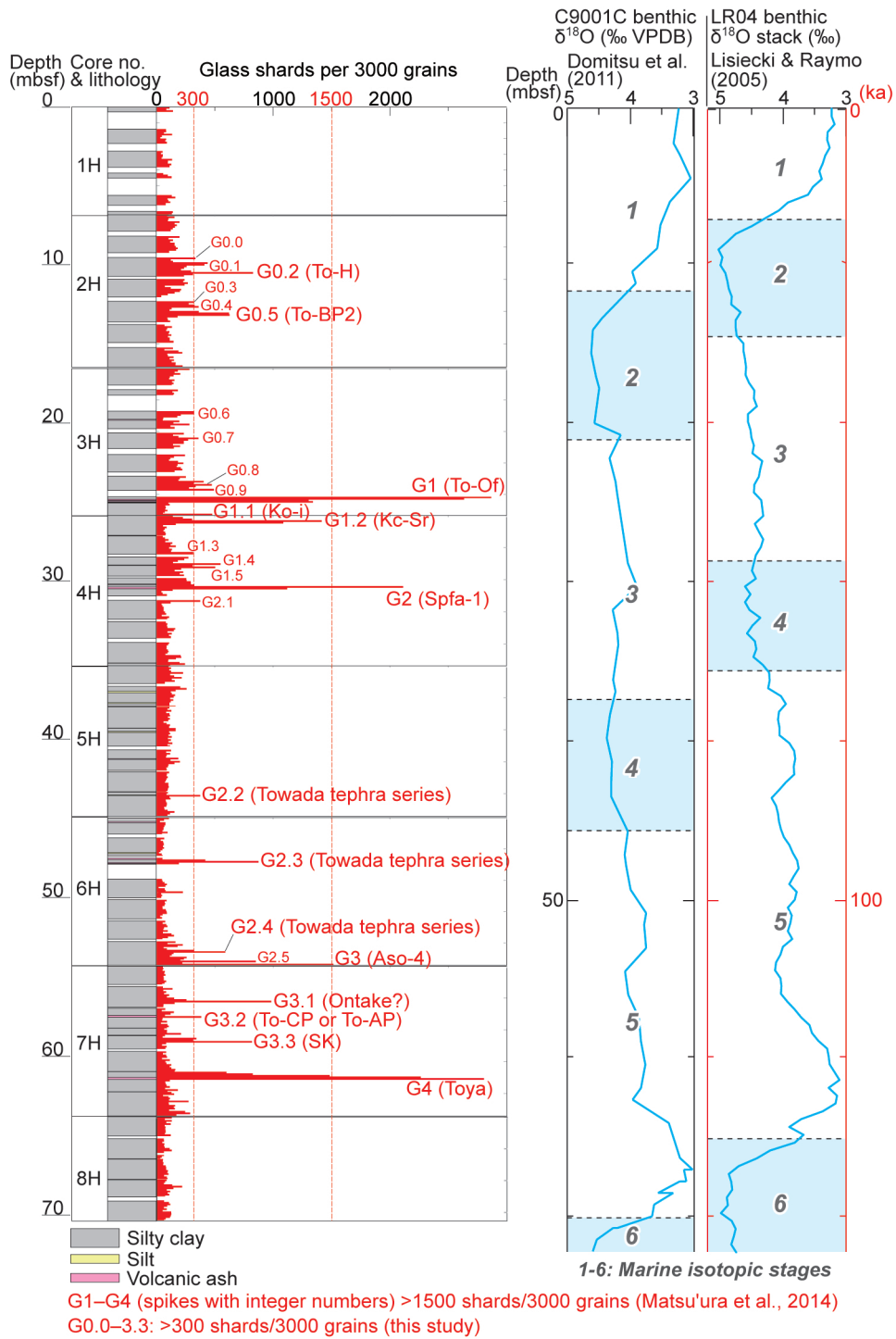


Fig. 2. Stratigraphy, tephra grain components, and oxygen isotopic record of benthic foraminifera in the C9001C cores. Core lithology and oxygen isotopic record are from Aoike (2007) and Domitsu et al. (2011), respectively. The LR04 benthic $\delta^{18}\text{O}$ stack is from Lisiecki and Raymo (2005). Tephra abbreviations (from older to younger): SK, Sambe-Kisuki; To-CP, Towada-Castera; To-AP, Towada-Aosuji; Spfa-1, Shikotsu-1; Kc-Sr, Kutcharo-Shoro; Ko-i, Komagatake-i; To-Of, Towada-Ofudo; To-BP2, Towada-Biscuit 2; To-H, Towada-Hachinohe.

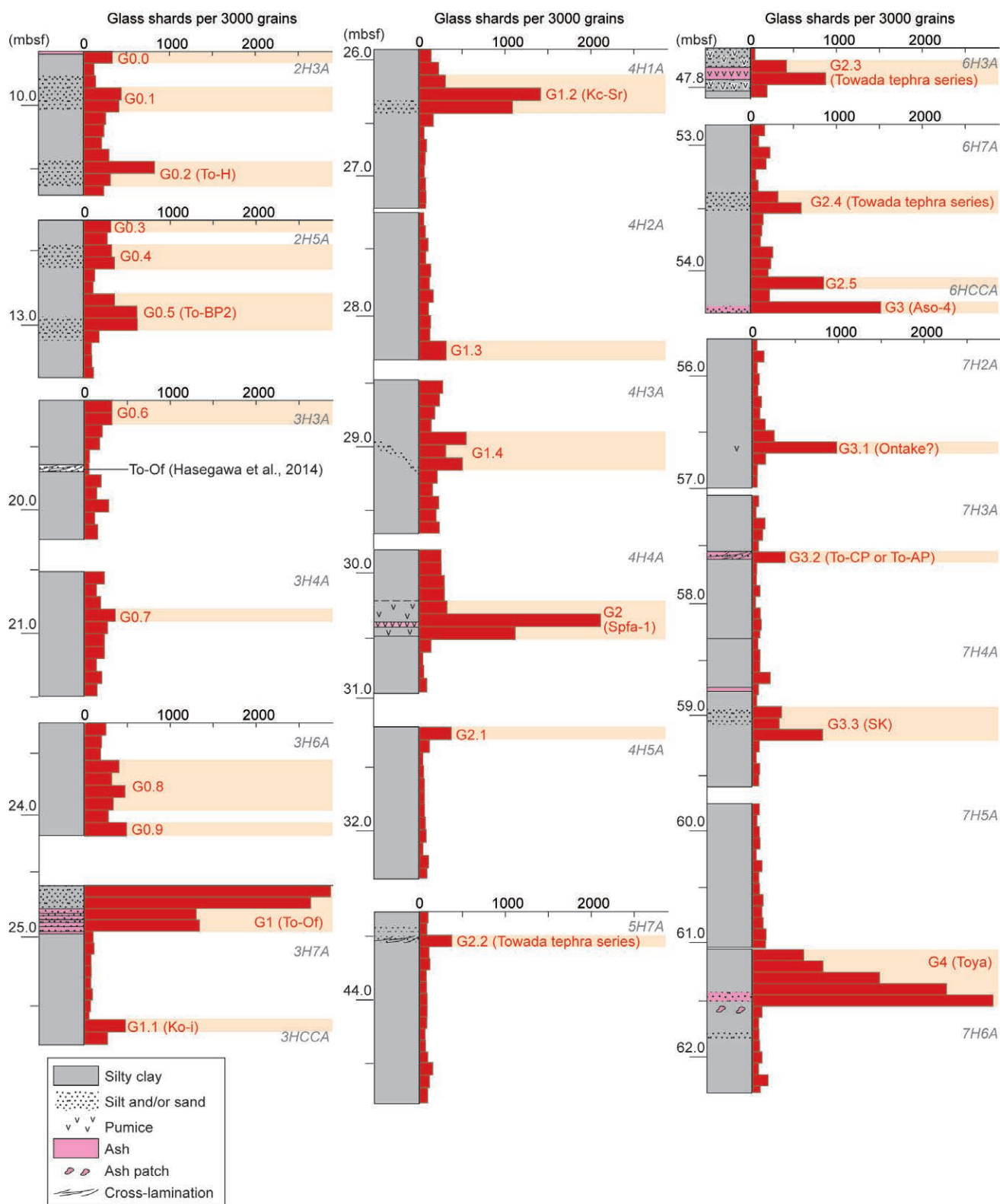


Fig. 3. Core lithology and tephra grain components corresponding to glass shard concentrations (spikes). Core lithology is based on our own core examination.

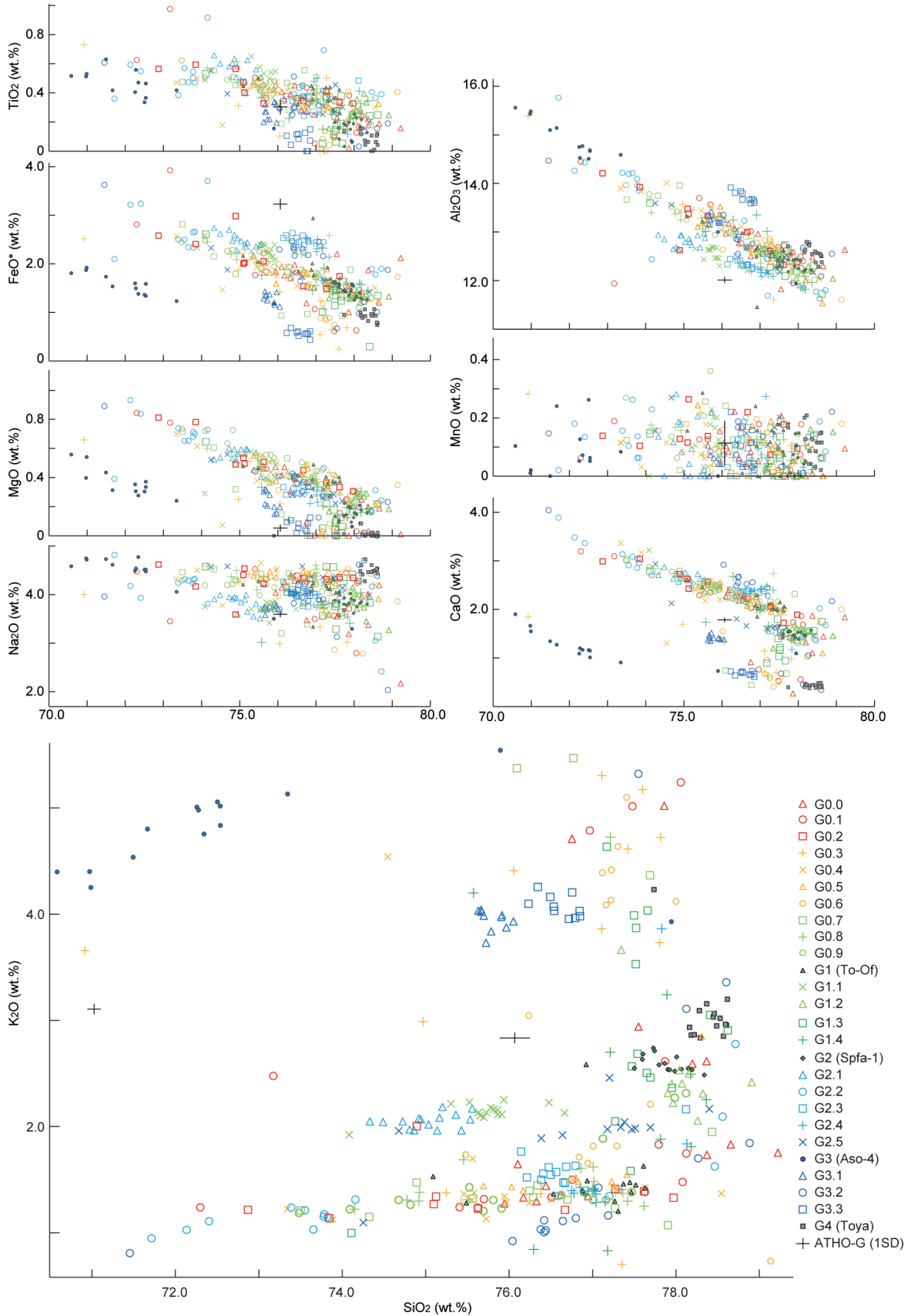


Fig. 4. Plots of major oxides against silica in glass shards from spikes G0.0–G4. Data of ATHO-G (a secondary standard glass provided by the Max Planck Institut fuer Chemie) were obtained in our laboratory.

328–362 shards. It corresponds to “silty clay” with an accessory description of “pumice scattering” in the VCD (Aoike, 2007). We confirmed this description by our core examination (Fig. 3). Shards had a wide SiO₂ range (73.4–78.6 wt.%) and low K₂O (1.1–1.7 wt.%), but one shard had high SiO₂ and K₂O (74.6 and 4.5 wt.%, respectively).

Spike G0.5 (12.87–13.17 mbsf, MIS 2) included 363–628 shards. It corresponds to “silty clay” with an accessory description of “pumice scattering” in the VCD (Aoike, 2007). We confirmed this description by our core examination (Fig. 3). Shards had wide-ranging SiO₂ (75.4–77.5 wt.%) and low K₂O (1.2–1.4 wt.%), but one shard had high SiO₂ and K₂O (78.6 and 3.0 wt.%, respectively).

Spike G0.6 (19.12–19.32 mbsf, MIS 2–3) included 322 shards. It corresponds to “silty clay” in the VCD, with no reported indication of an ash layer (Aoike, 2007). We confirmed this description by our core examination (Fig. 3). Shards fell into two groups according to their K₂O: a low-K₂O group (SiO₂ and K₂O contents, 75.1–77.8 wt.% and 1.3–2.0 wt.%, respectively) and a high-K₂O group (SiO₂ and K₂O, 77.2–78.2 wt.% and 4.3–5.6 wt.%, respectively). Two shards were outliers (SiO₂ and K₂O: 79.1 and 0.7 wt.%, respectively, and 76.0 and 3.0 wt.%, respectively).

Spike G0.7 (20.80–20.90 mbsf, MIS 3) included 361 shards. It corresponds to “silty clay” in the VCD, and no indication of an ash layer was reported (Aoike, 2007). We confirmed this description by our core examination (Fig. 3). Most of the shards had wide-ranging SiO₂ (73.5–78.4 wt.%) and low K₂O (1.1–2.0 wt.%). Three shards had high SiO₂ and K₂O (76.1–77.7 and 4.4–5.5 wt.%, respectively).

Spike G0.8 (23.55–23.95 mbsf, MIS 3) included 320–475 shards. It corresponds to “silty clay” in the VCD and no indication of an ash layer was reported (Aoike, 2007). We confirmed this description by our core examination (Fig. 3). Shards had a wide SiO₂ range (74.2–77.6 wt.%) and low K₂O (1.2–1.7 wt.%), but one shard had high SiO₂ and K₂O (77.2 and 4.7 wt.%, respectively).

Spike G0.9 (24.05–24.16 mbsf, MIS 3) included 493 shards. It corresponds to “silty clay” in the VCD, and no indication of an ash layer was reported (Aoike, 2007). We confirmed this description by our core examination (Fig. 3). Most of the shards had a wide SiO₂ range (73.5–77.5 wt.%) and low K₂O (1.2–1.4 wt.%). Three shards had high SiO₂ and moderate K₂O (77.1–78.1 and 1.9–2.3 wt.%, respectively).

Spike G1 (24.56–24.93 mbsf, late MIS 3) included

1304–2868 shards. It roughly corresponds to several ash and pumice layers in the VCD (Aoike, 2007). We observed interbeds of coarse-, fine-, and very fine grained ash layers, including pumice, with faint lamination (Fig. 3). Shards had high SiO₂ and low K₂O (75.1–77.6 and 1.2–1.4 wt.%, respectively), but one shard had high SiO₂ and moderate K₂O (76.9 and 2.6 wt.%, respectively). The shards have been identified as To-Of shards on the basis of their chemistry (Matsu'ura et al., 2014).

Spike G1.1 (25.64–25.74 mbsf, MIS 3) included 479 shards. It corresponds to “silty clay” in the VCD, with no indication of an ash layer (Aoike, 2007). We confirmed this description by our core examination (Fig. 3). Shards had high SiO₂ with low K₂O (75.3–76.7 and 2.1–2.3 wt.%, respectively), but one shard had high SiO₂ but lower K₂O (74.1 and 1.9 wt.%, respectively).

Spike G1.2 (26.11–26.41 mbsf, MIS 3) included 307–1416 shards. It corresponds to “silty clay” with an accessory description of “pumice scattering” in the VCD (Aoike, 2007).

We confirmed this description by our core examination (Fig. 3). Shards had high SiO₂ and low K₂O (77.9–78.9 and 2.1–2.5 wt.%, respectively), but one shard had high SiO₂ and K₂O (77.4 and 3.7 wt.%, respectively).

Spike G1.3 (28.18–28.33 mbsf, MIS 3) included 316 shards. It corresponds to “silty clay” in the VCD, with no indication of an ash layer (Aoike, 2007). We confirmed this description by our core examination (Fig. 3). Shards had a broad SiO₂ range (74.1–78.6 wt.%) and low K₂O (1.0–4.6 wt.%).

Spike G1.4 (28.89–29.19 mbsf, MIS 3) included 311–550 shards. It corresponds to a “glauconite-bearing pumiceous sandy silt” in the VCD (Aoike, 2007). We observed a sand pipe penetrating the silty clay, but we could not judge whether it represented a primary or secondary deformation structure (Fig. 3). Shards had a broad SiO₂ range (75.6–78.4 wt.%) and low K₂O (0.8–4.2 wt.%).

Spike G2 (30.21–30.51 mbsf, middle MIS 3) included 326–2114 shards. It roughly corresponds to a “sandy-silt-bearing pumiceous ash” reported at 30.30–30.39 mbsf by Aoike et al. (2007), who correlated it with the Spfa-1 tephra. We observed interbeds of clay with pumice (7 cm thick), pumice (4 cm thick), and clay with dense pumice (13 cm thick) in ascending order from 30.48 to 30.24 mbsf (Fig. 3). The upper contacts of the interbeds are unclear. Shards had high SiO₂ and moderate K₂O (77.5–78.3 and

2.5–2.7 wt.%, respectively), similar to the pyroclastic flow unit (Spfl) of Spfa-1. The shards have been identified by their chemistry as Spfa-1 shards (Matsu'ura et al., 2014).

Spike G2.1 (31.19–31.29 mbsf, MIS 3) included 376 shards. It corresponds to “silty clay” in the VCD, with no indication of an ash layer (Aoike, 2007). We confirmed this description by our core examination (Fig. 3). Shards had high SiO₂ and moderate K₂O (74.3–75.6 and 2.0–2.2 wt.%, respectively).

Spike G2.2 (43.49–43.58 mbsf, MIS 4) included 376 shards. It corresponds to a “dark grey glass-bearing fine sandy silt” in the VCD (Aoike, 2007). We observed interbeds of very fine sand and silt with cross-lamination (2.9 cm thick) at 43.51–43.54 mbsf (Fig. 3). Shards had a broad SiO₂ range (71.7–78.5 wt.%) and low K₂O (1.0–1.6 wt.%), but two shards had high SiO₂ and K₂O (78.6–78.7 and 2.1–2.8 wt.%, respectively).

Spike G2.3 (47.58–47.78 mbsf, MIS 5) included 420–876 shards. It corresponds to “silty clay” and “gray coarse pumice” in the VCD (Aoike, 2007). We observed interbeds of coarse sand- and silt-sized ash with pumice at 47.56–47.83 mbsf (Fig. 3). Shards had a broad range of SiO₂ (76.2–76.8 wt.%) and low K₂O (1.5–1.8 wt.%), but one shard had high SiO₂ and moderate K₂O (78.1 and 2.2 wt.%, respectively).

Spike G2.4 (53.35–53.53 mbsf, MIS 5) included 320–591 shards. It corresponds to “silty clay” in the VCD, with no indication of an ash layer (Aoike, 2007). We observed a 6.8-cm-thick silt layer at 53.44–53.51 mbsf within the silty clay (Fig. 3). Shards had a broad SiO₂ range (76.8–78.1 wt.%) and low K₂O (1.3–1.8 wt.%), but one shard had high SiO₂ and moderate K₂O (77.8 and 3.9 wt.%, respectively).

Spike G2.5 (54.04–54.14 mbsf, MIS 5) included 852 shards. It corresponds to “silty clay” in the VCD, with no reported indication of an ash layer (Aoike, 2007). We confirmed this description by our core examination (Fig. 3). Shards had a broad SiO₂ range (74.7–78.4 wt.%) and low K₂O (1.9–2.2 wt.%), but one shard had low K₂O (1.1 wt.%) and another had high K₂O (2.5 wt.%).

Spike G3 (54.24–54.34 mbsf, middle MIS 5) included 1517 shards. It corresponds to an “ash layer” reported at 54.35–54.38 mbsf by Aoike et al. (2010), who correlated it with the Aso-4 tephra. We observed a 5.5-cm-thick layer of silt-sized ash at 54.28–54.34 mbsf (Fig. 3). Its shards had broad ranges of SiO₂ and K₂O (63.3–

75.9 and 2.4–5.5 wt.%, respectively). One shard had an abnormally high SiO₂ and moderate K₂O (78.0 and 3.9 wt.%, respectively). The shards have been identified by their chemistry as Aso-4 shards (Matsu'ura et al., 2014).

Spike G3.1 (56.58–56.68 mbsf, MIS 5) included 983 shards. It corresponds to “silty clay” in the VCD, with no indication of an ash layer (Aoike, 2007). We observed a pumice particle with a 4-mm diameter at 56.63 mbsf within the silty clay (Fig. 3). Shards had a broad SiO₂ range (75.6–76.1 wt.%) and moderate K₂O (3.7–4.0 wt.%).

Spike G3.2 (57.55–57.65 mbsf, MIS 5) included 383 shards. It corresponds to a “dark gray and light gray sandy silt-bearing pumiceous clayey silt ash” in the VCD (Aoike, 2007). We observed an ash layer with cross-lamination (Fig. 3). Shards had a broad range of SiO₂ (71.5–78.9 wt.%) and low K₂O (0.8–1.8 wt.%), but three shards had high SiO₂ and high K₂O (77.6–78.6 and 3.1–5.3 wt.%, respectively).

Spike G3.3 (58.91–59.21 mbsf, MIS 5) included 315–818 shards. It corresponds to “silty clay” in the VCD, with an accessory description of “pumice scattering” (Aoike, 2007). We observed a 15-cm-thick fine sand-bearing silty clay layer at 58.93–59.08 mbsf (Fig. 3), but we did not observe the pumice scattering reported in the VCD. Further, the horizon with the largest shard concentration corresponded to silty clay, just below the sand-bearing clay layer. Shards had high SiO₂ and high K₂O (76.2–76.9 and 4.0–4.3 wt.%, respectively).

Spike G4 (61.05–61.55 mbsf, early MIS 5) included 599–2804 shards. It corresponds to a layer of “pumice and sandy silt-bearing and sandy silt-sized vitric ash” in the VCD (Aoike, 2007). We observed a 6.5-cm-thick layer of very fine silt-sized ash at 61.45–61.52 mbsf and also ash patches at about 61.55–61.58 mbsf (Fig. 3). Shards had high SiO₂ and moderate K₂O (78.2–78.6 and 2.8–3.2 wt.%, respectively). The shards have been correlated by their major-element chemistry with Toya shards (Matsu'ura et al., 2014).

5. Terrestrial tephtras potentially in the C9001C cores

In deep ocean settings, the isopach information based on the thickness of the tephra deposits is unreliable (Manville and Wilson, 2004; Allan et al., 2008). However, the possible offshore distribution of a terrestrial tephra on

the seafloor can be inferred by extrapolating the contours of an isopach map constructed from on-land data. In addition, ocean currents might transport tephra particles to distal areas beyond the 0-cm isopachs. We referred to published isopach maps and major ocean currents and tried to locate tephra from terrestrial sections that might potentially be found at the C9001C site. To-Of, Spfa-1, Aso-4, and Toya have been already correlated with the spikes G1, G2, G3, and G4, respectively, in the C9001C cores (Matsu'ura et al., 2014); other possible tephra are described below.

5.1 Kutcharo-Shoro tephra

Kutcharo-Shoro tephra (Kc-Sr) erupted from Kussharo volcano (Machida and Arai, 2003; Fig. 1) and forms a fallout ash layer on the Kushiro Plain. The isopach pattern of Kc-Sr is elongated eastward (Machida and Arai, 2003); therefore, the tephra was probably transported by the Oyashio Current to the C9001C drill site (Fig. 1b). Kc-Sr has been detected in other marine cores (MR98-03, PC-1, MR99-K04, PC-2 and PC-3 cores) from the northwestern Pacific Ocean floor (Aoki et al., 2000). In terrestrial loess deposits, Kc-Sr occurs above Spfa-1 and below an unidentified local tephra. Its thickness is 60 cm at location 1 (43.001361°N, 144.168806°E) (Fig. 5). Machida (1996) has reported on the sedimentary stratigraphy near location 1. In samples 101 and 102, which were collected by this study (Fig. 5), glass shards had high SiO₂ and moderate K₂O (77.9–78.9 and 2.1–2.5 wt.%, respectively; Fig. 6). The heavy mineral assemblage in both samples 101 and 102 consisted of orthopyroxene. Its eruptive age has been estimated as 40 cal ky BP by ¹⁴C dating and its stratigraphic relationship with other tephra (Yamamoto et al., 2010).

5.2 Komagatake-i tephra

Komagatake-i tephra (Ko-i) erupted from Komagatake volcano (Machida and Arai, 2003; Fig. 1) and occurs as fall and flow deposits along the Uchiura Bay coast. Although the isopach pattern of the fall deposits has not yet been clarified, fall and flow deposits with thicknesses of ~120 cm and >10 m, respectively, are widely observed to the east of Komagatake volcano (Yoshimoto et al., 2008). Hasegawa et al. (2014) suggested that Ko-i is correlated with an ash layer at 25.5 mbsf in the C9001C cores. In terrestrial deposits, Ko-i occurs above Numajiri debris avalanche deposits and below deposits of an unidentified debris avalanche. Ko-i fall and pyroclastic flow deposits

are 120 cm and 4–5 m thick, respectively, at location 2 (42.092050°N, 140.769128°E) (Fig. 5). The stratigraphy near location 2 has been reported by Yoshimoto et al. (2008). Glass shards in samples 201 and 202, collected from the fall and flow deposits, respectively, by this study (Fig. 5), had high SiO₂ and moderate K₂O contents (sample 201, 75.5–76.4 and 2.1–2.3 wt.%, respectively; sample 202, 75.8–77.2 and 2.1–2.3 wt.%, respectively) (Fig. 6). The heavy-mineral assemblage in both samples 201 and 202 consisted of orthopyroxene with a small amount of clinopyroxene. Its eruption age has been estimated as 39 cal ky BP by ¹⁴C dating (Yoshimoto et al., 2008).

5.3 Towada-Biscuit 2 tephra

Towada-Biscuit 2 tephra (To-BP2) erupted from Towada volcano (Machida and Arai, 2003; Fig. 1) and forms fallout ash and pumice layers on the Kamikita Plain. To-BP2 has been identified as a tephra above the Towada-Biscuit 1 tephra (To-BP1), which is a basal fall tephra that underlies To-Of pyroclastic flow deposits (Machida and Arai, 2003). To-BP2 isopach distributions have not yet been reported. At locations 3 (40.534472°N, 141.141361°E) and 4 (40.587222°N, 141.434167°E), To-BP2 occurs above To-Of and below Towada-Hachinohe tephra (described below) in loess deposits. Its thickness is 26 cm at location 3 and 30 cm at location 4 (Fig. 5). The stratigraphy at location 3 has been reported by Kudo and Kobayashi (2013). Glass shards in samples 302, 303, 402, and 403, obtained by this study (Fig. 5), had a broad SiO₂ range (73.1–78.4 wt.%) and low K₂O (1.2–1.5 wt.%) (Fig. 6). The heavy-mineral assemblage in samples 302, 303, 402 and 403 consisted of orthopyroxene. The eruption age of To-BP2 has been estimated to be slightly younger than 20.8–21.5 cal ky BP on the basis of the ¹⁴C age of humic sediments just below To-BP2 (Kudo and Kobayashi, 2013).

5.4 Towada-Hachinohe tephra

Towada-Hachinohe tephra (To-H) erupted from Towada volcano (Machida and Arai, 2003; Fig. 4) and forms fallout ash and pumice layers on the Kamikita Plain. The isopach pattern of the basal fall unit that underlies the To-H pyroclastic flow deposits, referred to as To-HP, is elongated toward the northeast (Machida and Arai, 2003). Therefore, it may extend to the C9001C drill site. To-H (To-HP) occurs above the To-BP2 tephra in loess deposits, and its thickness is 135 cm at location 3 and 190 cm at location 4 (Fig. 5).

Glass shards in samples 304 and 404 had a wide range of SiO₂ (73.9–76.6 wt.%) and low K₂O (1.0–1.4 wt.%) (Fig. 6). The heavy-mineral assemblage in both samples 304 and 404 consisted of orthopyroxene and amphibole. The eruption age of To-H is 14.9–15.3 ka from the δ¹⁸O stratigraphy of deep-sea sediments (Aoki and Arai, 2000).

5.5 Ontake-Pumice 1 tephra

Ontake-Pumice 1 tephra (On-Pm1) erupted from Ontake volcano (Machida and Arai, 2003; Fig. 1) and forms a fallout pumice layer in the area downwind of the volcano. Its isopach pattern is elongated toward the northeast (Machida and Arai, 2003), and it may extend to the C9001C drill site. On-Pm1 occurs below Ontake-Shiojiri Pumice (SoP) in loess deposits (Suzuki, 1996), and its thickness is 70 cm at location 5 (Fig. 5). Glass shards in sample 501, obtained by this study, had high SiO₂ and moderate K₂O (75.5–76.1 and 3.5–3.7 wt.%; Fig. 6). The heavy-mineral assemblage in sample 501 consisted of very small amounts of amphibole and orthopyroxene. Its eruption age has been estimated by δ¹⁸O stratigraphy as MIS 5c (Aoki et al., 2008).

5.6 Sambe-Kisuki tephra

Sambe-Kisuki tephra (SK) erupted from Sambe volcano (Machida and Arai, 2003; Fig. 1) and forms fallout pumice layers in the area downwind of the volcano. Its isopach pattern is elongated toward the northeast (Machida and Arai, 2003), and it may extend to the C9001C drill site. It occurs below Sambe-Un'nan tephra (SUn), and its thickness is 198 cm at location 6 (35.216383°N, 133.067072°E) (Fig. 5). Glass shards in samples 601–604, obtained by this study, had high SiO₂ and moderate K₂O (76.6–77.2 and 3.8–4.4 wt.%, respectively; Fig. 6). The heavy-mineral assemblage in samples 601–604 consisted of amphibole. Its eruption age has been estimated as MIS 5c on the basis of its stratigraphic relationship with other tephras (Machida and Arai, 2003).

6. Discussion

6.1 Correlation of tephras by glass shard major element chemistry

6.1.1 Spikes G0.0–G0.9 and G1 (To-Of)

Spikes G0.0–G0.9 are glass shard spikes

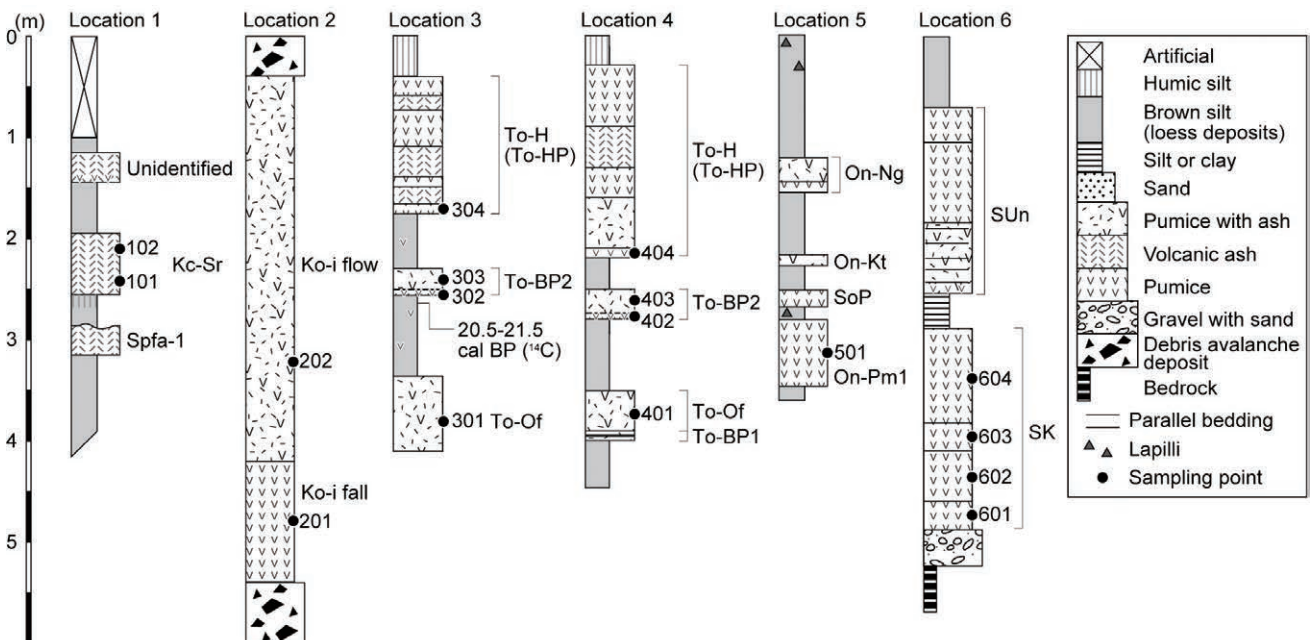


Fig. 5. Stratigraphic columns of tephras in loess deposits. Locations of outcrops are shown in Fig. 1a and 1b. The ¹⁴C age below To-BP2 at Location 3 is from Kudo and Kobayashi (2013). Tephra abbreviations not shown in Figure 2: On-Ng, Ontake-Nagawa; On-Kt, Ontake-Katamachi; SoP, Ontake-Shiojiri Pumice; On-Pm1, Ontake-Pumice 1; SUn, Sambe-Un'nan; To-HP, Towada-Hachinohe Pumice (the basal fall unit underlying the To-H pyroclastic flow deposits).

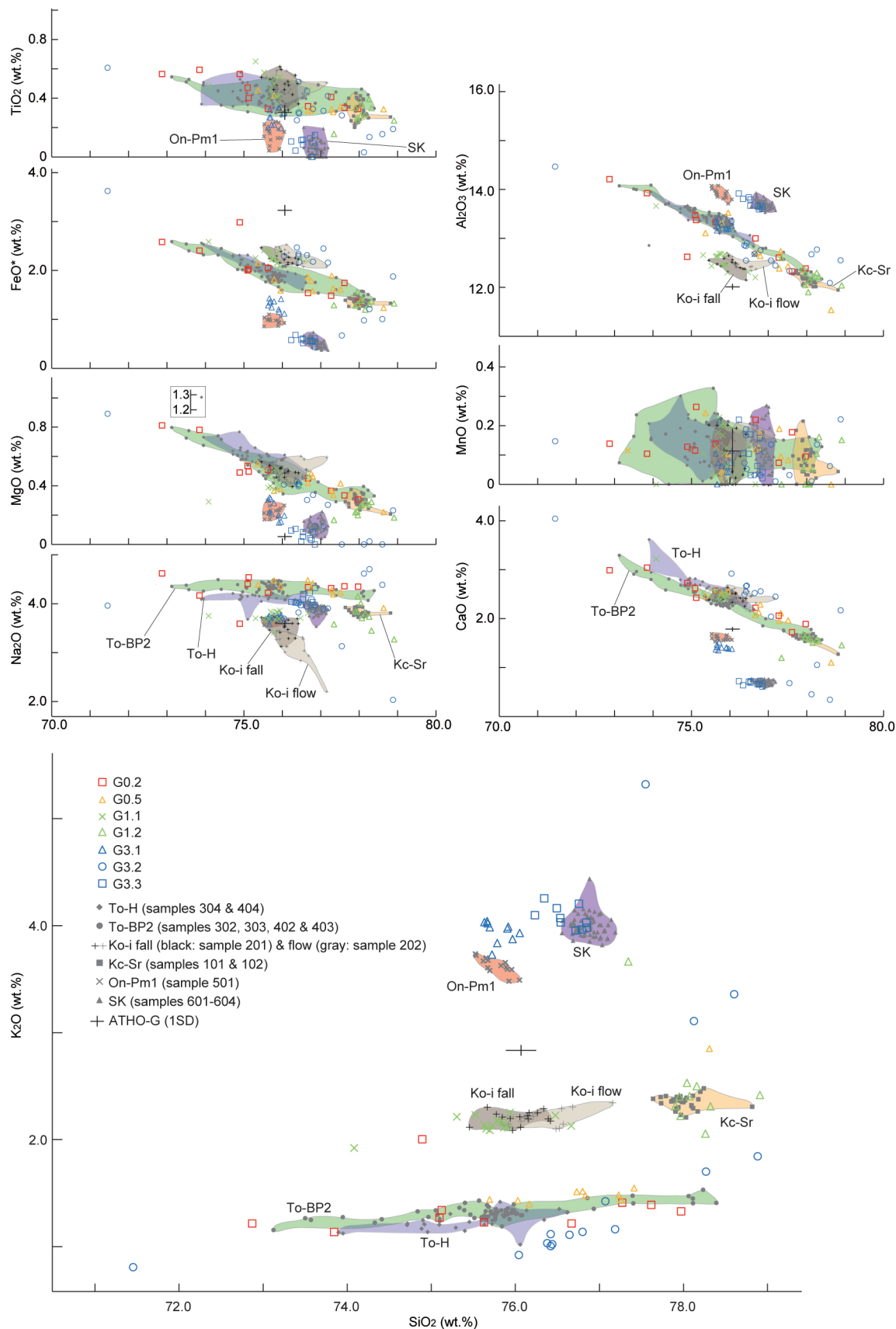


Fig. 6. Plots of major oxides against silica in glass shards from selected spikes and correlative tephras. Data of ATHO-G (a secondary standard glass provided by the Max Planck Institut fuer Chemie) were obtained in our laboratory.

stratigraphically above spike G1 (To-Of, middle MIS 3; Matsu'ura et al., 2014) in the C9001C cores. The shards, like the To-Of shard population, usually had a broad SiO₂ range (72–79 wt.%) and low K₂O (1–2 wt.%). This shard chemistry indicates that spikes G0.0–G0.9 are tephra from Towada volcano or, possibly, reworked deposits of tephra younger than To-Of.

In the tephrostratigraphy in loess downwind of Towada volcano, To-H and To-BP2 are above To-Of (Machida and Arai, 2003). The eruption age of To-H has been estimated as 14.9–15.3 ka from the $\delta^{18}\text{O}$ stratigraphy of deep-sea sediments (Aoki and Arai, 2000), whereas that of To-BP2 must be slightly younger than 20.5–21.5 cal ky BP, based on the ¹⁴C age of humic sediments just below To-BP2 on the Kamikita Plain (Kudo and Kobayashi, 2013). Therefore, To-H and To-BP2 may correlate with two of spikes G0.0–0.9.

The shard chemistries of To-H and To-BP2 were characterized by broad SiO₂ content ranges (73.9–76.6 and 73.1–78.4 wt.%, respectively) and low K₂O (1.0–1.4 and 1.2–1.5 wt.%, respectively). These chemistries are similar to the To-Of chemistry because all three tephra originated from Towada volcano.

Among spikes G0.0–G0.9, spikes G0.2 and G0.5 included 828 and 628 shards, thus forming clear tephra horizon spikes. Further, these two spikes correspond to the MIS 2 to 1 transition (ca. 15 ka), just after the coldest period in MIS 2 (ca. 18 ka) (Fig. 2). These shard abundances and estimated stratigraphic ages indicate that spikes G0.2 and G0.5 likely correlate with To-H and To-BP2, respectively (Fig. 7). In the deep-sea sediments of the C9001C cores, therefore, To-H and To-BP2 are cryptotephra, not visible layers, and they are reported for the first time by this study.

6.1.2 Spikes G1.1–G1.4 and G2 (Spfa-1)

Spikes G1.1–G1.4 are glass shard spikes between To-Of (MIS 3) and Spfa-1 (spike G2, middle MIS 3; Matsu'ura et al., 2014). Shards of spikes G1.1 and G1.2 had moderate K₂O (2.1–2.5 wt.%), and shards of spikes G1.3 and G1.4 had a broad K₂O range (1.6–4.6 wt.%). These shard chemistries are thus different from the low-K₂O shards of spikes G0.0–G0.9 and G1.

Spike G1.1 has not previously been correlated with any tephra. Hasegawa et al. (2014) reported a thin, 5-mm-thick tephra layer at 25.5 mbsf, very close to the depth of the spike G1.1 horizon, and they suggested it might correlate

with Ko-i. In our terrestrial samples, shards of Ko-i fall and flow deposits had high SiO₂ and moderate K₂O, similar to the shard chemistry of spike G1.1 (Fig. 6). Further, because the Na₂O of the Ko-i fall deposit is more similar than that of the Ko-i flow deposit to the Na₂O content of the G1.1 shards, spike G1.1 likely corresponds to the Ko-i fall deposit.

The shard chemistries of spike G1.2 and Kc-Sr are similar. Further, spike G1.2 dates to mid-MIS 3 (ca. 40 ka) in the $\delta^{18}\text{O}$ stratigraphy of the C9001C cores. This stratigraphic age of spike G1.2 is in accordance with the reported age of Kc-Sr (35–40 ka; Machida and Arai, 2003); therefore, spike G1.2 is correlated with Kc-Sr (Fig. 7). Marine tephrostratigraphy off NE Japan indicates that Kutcharo-Shoro (Kc-Sr) occurs between To-Of and Spfa-1 (Aoki et al., 2000). Thus, spike G1.2 likely correlates with Kc-Sr.

Spikes G1.3 and G1.4 are classified as reworked tephra because the broad K₂O range of their shards indicates contamination from multiple sources.

6.1.3 Spikes G2.1–G2.5 and G3 (Aso-4)

Spikes G2.1–G2.5 are glass shard spikes between Spfa-1 (spike G2, MIS 3) and Aso-4 (spike G3, MIS 5b; Aoki, 2008; Matsu'ura et al., 2014). Shards of spikes G2.2, G2.3, and G2.4 had a broad SiO₂ range and low K₂O, similar to shards of the Towada tephra series found in stratigraphically higher positions (To-H, To-BP2, and To-Of). Different from the Towada tephra series, however, spikes G2.1 and G2.5 had high SiO₂ and moderate K₂O.

The reported tephrostratigraphy of Towada volcano between Aso-4 and To-Of is as follows: in ascending order, Towada-T17 (To-T17), Towada-QP (To-QP), Towada-Okoshi (To-Ok2), Towada-Red (To-Rd), Towada-Okuse (To-Os), Towada-Kibidango (To-Kb), and Towada-Godo (To-G) (Machida and Arai, 2003). Some of these tephra are probably correlated with spikes G2.2, G2.3, and G2.4 (Fig. 7), but it is difficult to discriminate them because of the similarity of their shard chemistries.

Spikes G2.1 and G2.5 have not previously been correlated with any tephra. We cannot yet correlate spike G2.1 with any reported tephra. Spike G2.5, situated just above spike G3 (Aso-4), cannot be reworked deposits of Aso-4 because the shard chemistry of the spike differs from that of Aso-4. Alternatively, spike G2.5 might correlate with a tephra at 52.8 mbsf (just above Aso-4), postulated to be Kt-6 or Kt-7 (Aoki et al., 2012). However, Na₂O and

K₂O of spike G2.5 (4.0–4.6 and 1.9–2.2 wt.%, respectively) differ from reported Na₂O and K₂O of both Kt-6 (3.62 ±0.2 and 1.52 ±0.2 wt.%, respectively) and Kt-7 (3.60 ±0.2 and 1.36 ±0.4 wt.%, respectively) (Aoki and Machida, 2006). Therefore, we cannot correlate spike G2.5 with any reported tephra. Although spike G2.4 is situated 50 cm above spike G2.5, it cannot have formed by the reworking of spike G3 or G2.5, because their shard chemistries are distinct. Therefore, spikes G3, G2.5, and G2.4 represent three closely timed individual eruptions during MIS 5b to 5a.

6.1.4 Spikes G3.1–G3.3 and G4 (Toya)

Spikes G3.1–G3.3 are glass shard spikes between Aso-4 (spike G3, MIS 5b) and Toya (spike G4, MIS 5d; Matsu'ura et al., 2014). Shard chemistries of spikes G3.1, G3.2, and G3.3, and G4 were all different from each other; thus, each is an individual tephra.

The tephrostratigraphy between Toya and Aso-4 in northern Honshu includes SK (MIS 5c), On-Pm1 (MIS 5c), Dokusawa (Dks, MIS 5b–5c), Towada-Aosuji (To-AP, MIS 5b–5d), and Towada-Castera (To-CP, MIS 5b–5d) in

ascending order (Machida and Arai, 2003; Matsu'ura et al., 2011).

The shard chemistry of spike G3.1 is similar to that of On-Pm1 with respect to SiO₂, TiO₂, MnO, and Na₂O (Fig. 6). However, with respect to Al₂O₃, CaO, and K₂O their chemistries only partially overlap. Therefore, although spike G3.1 may have possibly originated from Ontake volcano (Fig. 7), the correlation between spike G3.1 and the Ontake tephra series requires further study.

The shards of spike G3.2 had low K₂O (0.8–1.8 wt.%), suggesting that the spike belongs to the Towada tephra series such as To-CP or To-AP. Both of these tephras may reach the C9001C drill site, as inferred from their reported isopach maps (Machida and Arai, 2003). Because we have not yet confirmed a difference in shard chemistry between To-AP and To-CP, we have not correlated spike G3.2 with either To-CP or To-AP (Fig. 7).

The shards of spike G3.3 had high K₂O (4.0–4.3 wt.%), similar to SK shards. Thus, we consider spike G3.3 to correlate with SK (Fig. 7). Machida and Arai (2003) placed SK in MIS 5c by its stratigraphic position relative to other

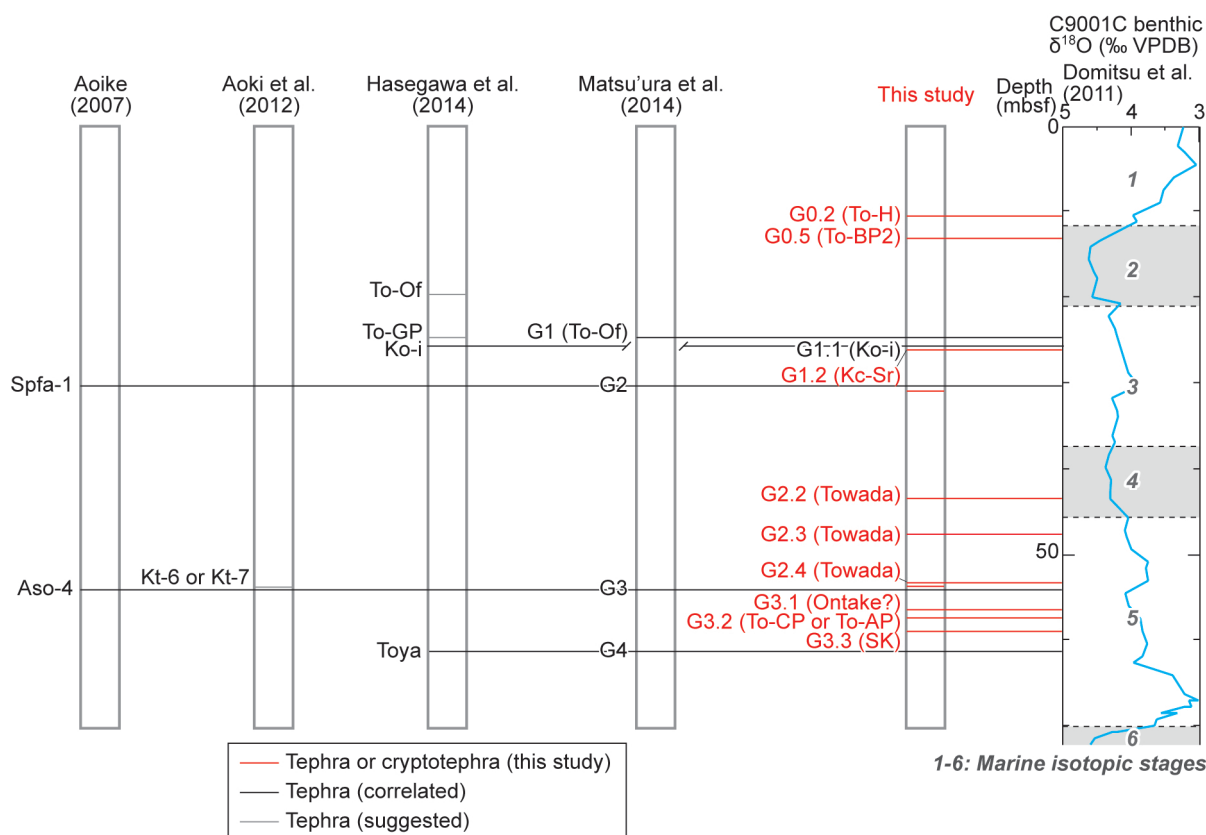


Fig. 7. Correlations of Late Pleistocene tephras in the C9001C cores. Tephra abbreviations not shown in previous figures: To-GP, Towada-Godo; Kt-6, Kuttara 6; Kt-7, Kuttara 7.

well-dated widespread tephra. In this study, the SK tephra is placed in the MIS sequence by direct evidence for the first time.

6.2 Relationship between core lithology and glass shard abundance

6.2.1 Verification of tephra layers in the VCD

Visible tephra layers were reported at 18 horizons in the Late Pleistocene sediments (1H–mid 8H cores) in the VCD (Table 3). Seven of these tephra layers are associated with the recognized spikes of this study. On the basis of glass chemistry, six out of the seven tephra layers correspond to spikes G1, G2, G2.3, G3, G3.2, and G4 (Fig. 7; Table 2). Therefore, most tephra layers in the VCD that correspond to spikes provide reliable information about tephra horizons. Only the tephra layer corresponding to spike G0.0 has been classified as reworked (see Section 6.2.2).

Some crystal-rich tephra layers may not be identifiable by glass shard abundance; therefore, some reported tephra layers in the VCD were not detected. For example, the tephra layer reported at 19.64–19.71 mbsf in the VCD, which has been correlated with To-Of (Hasegawa et al., 2014) (Fig. 3), includes only 55 glass shards and thus does not show up as a glass shard spike. However, To-Of pyroclastic flow and fall deposits in terrestrial sediments (samples 201 and 301) are glassy, including 1015–1938 shards per 3000 grains. Therefore, we have difficulty with the correlation of this layer with To-Of. Moreover, Matsu'ura et al. (2014) successfully correlated spike G1 (24.56–24.93 mbsf) with To-Of instead, and the stratigraphic age of G1 (late MIS 3; Fig. 2) is consistent with the reported age of To-Of (Machida and Arai, 2003). Further, in our core examination, we determined the layer at 19.64–19.71 mbsf in the VCD to be a sand layer, not a tephra layer; therefore, we suggest that this layer is an example of an over-recorded tephra layer in the VCD (Mahony et al., 2014).

Although spikes G0.2, G0.5, G1.2, G2.2, G2.4, and G3.3 did not correspond to tephra layers in the VCD (Aoiike, 2007: Section 6.1), they are associated with non-tephra layers with tephra-related descriptions such as “glass-bearing” or “pumice scattering”. Such descriptions may imply the presence of a cryptotephra. However, only six out of 65 VCD-based non-tephra horizons corresponded to glass shard spikes (Table 3). Therefore, it is hard to consider such descriptions as an indicator of a cryptotephra horizon.

Spikes G0.2 (To-H), G0.5 (To-BP2), and G2.4

(Towada tephra series) are cryptotephra; they do not correspond to tephra layers in the VCD, nor could we detect them in our core examination. Spikes G2.2, G2.3, and G3.2 (all Towada tephra series) are visible tephra layers in the VCD and our core examination, but not all tephra layers originated from Towada volcano were found to form visible tephra layers in the cores. Most of Late Pleistocene tephra layers derived from Towada volcano should be able to form visible layers in the cores because the reported isopach distributions of terrestrial deposits (Machida and Arai, 2003) can be extrapolated to the C9001C drill site. Thus, whether or not a marine tephra is preserved as a tephra layer depends on the depositional and post-depositional processes to which it is subjected (Lowe, 2011), not simply on the eruptive volume or distance from the source (Manville and Wilson, 2004; Allan et al., 2008). Since a marine tephrostratigraphy constructed only from visible tephra layers has large gaps compared with the terrestrial tephrostratigraphy, glass shard spikes (cryptotephra) have significant potential to improve the marine tephrostratigraphy (Fig. 7). Therefore, it is important to examine all glass shard spikes and verify correlations to the land sections in terms of glass chemistry and mineral assemblage. For crystal-rich tephra layers, mineral assemblage and chemistry can be used as an alternative means of correlation (e.g., Matsu'ura and Komatsubara, 2015).

6.2.2 Interpretation of vertical glass shard profiles to infer transport and depositional processes

Tephra layers in deep-sea sediments sometimes show cross-lamination, which is an indication that the tephra particles were laterally transported by bottom currents (Griggs et al., 2014). If remobilized tephra particles form a reworked layer at an upper (younger) horizon from the true stratigraphic position, serious chronological uncertainty can result. This problem is a critical concern in not only tephrostratigraphy but also cryptotephrostratigraphy.

Spikes G0.0 and G0.1, which are stratigraphically above To-H (spike G0.2), include many glass shards of To-H together with small amounts of glass shards from other tephra layers (Fig. 4; Section 6.1). However, the total shard number of spike G0.1 (sum of samples no. 58 and 59) is 852, roughly equal to the shard number (828) in sample no. 64 of spike G0.2 (Table 2). The To-H shards might be diluted by those of another tephra. If spike G0.1 is correlated with To-H, then spike G0.2 would have to be an individual

Table 2. Glass shard spikes (G0.0–4), number of shards per 3000 grains, and correlative tephra in the C9001C cores. Information on spikes G1, 2, 3, and 4 is from Matsu'ura et al. (2014).

Sample number	Horizon in core (*, EDS analyzed)	Depth (mbsf)	Glass shards (/3000 grains)	Spike ID	Tephra
55	2H3A0-10*	9.56-9.66	336	G0.0	Reworked
58	2H3A30-40*	9.86-9.96	440	G0.1	Reworked
59	2H3A40-50	9.96-10.06	412		
64	2H3A90-100*	10.46-10.56	828	G0.2	Towada-Hachinohe (To-H)
65	2H3A100-110	10.56-10.66	314		
78	2H5A0-10*	12.27-12.37	320	G0.3	Reworked
80	2H5A20-30	12.47-12.57	328	G0.4	Reworked
81	2H5A30-40*	12.57-12.67	362		
84	2H5A60-70	12.87-12.97	363	G0.5	Towada-Biscuit 2 (To-BP2)
85	2H5A70-80	12.97-13.07	623		
86	2H5A80-90*	13.07-13.17	628		
130	3H3A0-10	19.12-19.22	322	G0.6	Reworked
131	3H3A10-20*	19.22-19.32	322		
144	3H4A30-40*	20.80-20.90	361	G0.7	Reworked
165	3H6A30-40	23.55-23.65	405	G0.8	Reworked
166	3H6A40-50	23.65-23.75	320		
167	3H6A50-60*	23.75-23.85	475		
168	3H6A60-70	23.85-23.95	337		
170	3H6A80-91*	24.05-24.16	493	G0.9	Reworked
171	3H7A0-10*	24.56-24.65	2868	G1	Towada-Ofudo (To-Of)
172	3H7A10-20	24.65-24.74	2636		
173	3H7A20-30	24.74-24.83	1304		
174	3H7A30-40	24.83-24.93	1342		
183	3HCCA0-10*	25.64-25.74	479	G1.1	Komagatake-i (Ko-i)
187	4H1A20-30	26.11-26.21	307	G1.2	Kutcharo-Shoro (Kc-Sr)
188	4H1A30-40*	26.21-26.31	1416		
189	4H1A40-50	26.31-26.41	1088		
208	4H2A100-115*	28.18-28.33	316	G1.3	Reworked
213	4H3A40-50*	28.89-28.99	550	G1.4	Reworked
214	4H3A50-60	28.99-29.09	311		
215	4H3A60-70	29.09-29.19	505		
225	4H4A40-50	30.21-30.31	326	G2	Shikotsu-1 (Spfa-1)
226	4H4A50-60*	30.31-30.41	2114		
227	4H4A60-70	30.41-30.51	1120		
232	4H5A0-10*	31.19-31.29	376	G2.1	Undifferentiated
349	5H7A20-30*	43.49-43.58	376	G2.2	Towada tephra series
387	6H3A10-20	47.58-47.68	420	G2.3	Towada tephra series
388	6H3A20-30*	47.68-47.78	876		
432	6H7A60-70	53.35-53.44	320	G2.4	Towada tephra series
433	6H7A70-80*	53.44-53.53	591		
440	6HCCA0-10*	54.04-54.14	852	G2.5	Undifferentiated
442	6HCCA20-29.5*	54.24-54.34	1517	G3	Aso-4
464	7H2A90-100*	56.58-56.68	983	G3.1	Ontake?
473	7H3A50-60*	57.55-57.65	383	G3.2	Towada-Castera (To-CP) or Towada-Aosuji (To-AP)
487	7H4A60-70	58.91-59.01	341	G3.3	Sambe-Kisuki (SK)
488	7H4A70-80	59.01-59.11	315		
489	7H4A80-90*	59.11-59.21	818		
507	7H6A0-10	61.05-61.15	599	G4	Toya
508	7H6A10-20	61.15-61.25	824		
509	7H6A20-30	61.25-61.35	1483		
510	7H6A30-40	61.35-61.45	2263		
511	7H6A40-50*	61.45-61.55	2804		

tephra from Towada volcano below To-H and above To-BP2. However, the occurrence of a tephra between To-H and To-BP2 is not suggested by the on-land tephrostratigraphy (Fig. 5), and no such tephra has been reported (Machida and Arai, 2003). Therefore, we interpreted spike G0.1 as not correlated with To-H but classified it as reworked To-H. Further, spike G0.0 also represents reworked To-H because it includes similar glass shards to spike G0.1. Spike G0.0 (a visible ash layer) is stratigraphically above spike G0.1. These tephra materials that experienced repeated reworking do not display a simple decreasing-upward depositional profile.

Similarly, spikes G0.3 and G0.4 above To-BP2, and spikes G0.6–G0.9 above To-Of (spike G1) were also inferred to be the result of repeated reworking following huge Towada volcano eruptions (Fig. 3).

Spikes G1.3 and G1.4 occur above spike G2 (Spfa-1). Although the chemistry of some shards of the spikes is similar to the Spfa-1 chemistry, many shards do not cluster with the Spfa-1 population. Therefore, we interpreted spikes G1.3 and G1.4 to have resulted from post-depositional mixing of Spfa-1 with glass shards from other tephtras.

The shard chemistry of spike G2.2 suggests that this spike consists of tephra derived from Towada volcano (Fig. 3) and it correlates with MIS 4 (Fig. 7). This spike, as well as spike G3.2 (To-CP or To-AP), occurs in sediment showing cross-lamination. Cross-lamination in marine sediments is lithological evidence for secondary deposition by bottom currents, but it can represent almost no time delay or considerable time delay after the tephra eruption. Here, the stratigraphic position of spike G3.2 (MIS 5c) is in accordance with the terrestrial tephrostratigraphy. Therefore, the time between the eruption and the deposition of the tephra was short and does not affect the integrity

of the marine tephrostratigraphy. Spike G2.2, like other Towada volcano-derived tephtras such as spikes G0.2 (To-H) and G3.3 (To-CP or To-AP), shows a broad SiO₂ range, but there is no clear indication of a shard mixture reflecting contamination from various sources (Fig. 4). Therefore, it is likely an individual tephra, not a reworked tephra.

Glass shards above spikes G3.3 (SK) and G4 (Toya) gradually decrease upward in number (Fig. 3). This upward decrease indicates immediate reworking, that is, just after emplacement of the shards on the seafloor, and suggests bioturbation or winnowing by bottom currents. It is feasible that this occurred during the interstadial conditions that followed their primary deposition onto the seafloor (Griggs et al., 2014). Because the spike G3.3, the glass shard peak, does not correspond to the base of the fine sand-bearing clay layer, determination of the primary depositional horizon of this cryptotephra is still problematic. However, the gap between the shard spike and the visible layer base is less than 10 cm; therefore, it does not cause serious uncertainty in the stratigraphic position of the SK tephra (MIS 5c: Fig. 7). Spike G4 corresponds to an ash layer with underlying ash patches (Fig. 3). The presence of discrete tephra patches suggests that glass shards have become mixed with the underlying sediment. This mixing may have resulted either from gravitational loading or from bioturbation. However, because the ash patches are near the Toya base (within 10 cm), the secondary deformation does not introduce serious uncertainty into the stratigraphic position of Toya tephra (MIS 5d: Fig. 7).

By using the glass shard profile, we were able to detect tephtras and cryptotephtras not previously reported. Further, we were able to confirm whether their stratigraphic positions preserved chronological integrity even in the case of upward or downward dissemination of some glass shards.

Table 3 Number of tephra layers and number of sediment horizons with tephra-related descriptions in each segment of the Late Pleistocene sediments in the visual core description (VCD) (Aoike, 2007).

The number of layers or horizons with corresponding glass shard spikes in each segment is shown in parentheses. * The boundary between the Middle and the Late Pleistocene (MISs 6 and 5) is at 69.97 mbsf in the 8H core segment (Domitsu et al., 2011).

Late Pleistocene segment	No. of tephra layers in VCD (no. with corresponding spikes)	No. of sediment horizons with tephra-related description in VCD (no. with corresponding spikes)
1H	0 (0)	2 (0)
2H	1 (1)	9 (3)
3H	5 (1)	7 (0)
4H	4 (1)	16 (1)
5H	1 (0)	16 (1)
6H	4 (2)	8 (0)
7H	3 (2)	7 (1)
8H*	0 (0)	0 (0)

Therefore, glass shard profiling has significant potential for construction and improvement of marine tephrostratigraphy.

7. Conclusion

We investigated the Late Pleistocene deep-sea core samples from the C9001C drill site to refine the regional tephrostratigraphy. We first counted the glass shards in contiguous marine core sediment samples, and then analyzed the major element chemistry of glass shards from 26 spikes. These spikes corresponded to four previously reported tephras (G1, G2, G3, and G4 from top to bottom), three newly identified visible tephras, and 19 newly identified non-visible tephras (cryptotephras) (G0.0–0.9, G1.1–1.4, G2.1–2.5, and G3.1–3.3). Our main findings are as follows:

(1) We newly correlated Spike G0.2 with the Towada-Hachinohe (To-H: MIS 1/2, 15 ka), G0.5 with the Towada-Biscuit 2 (To-BP2: MIS 2, 18 ka), G1.1 with the Komagatake-i (Ko-i: 39 ka), G1.2 with the Kutcharo-Shoro (Kc-Sr: MIS 3, 40 ka), and G3.3 with the Sambe-Kisuki (SK: MIS 5c, 100 ka) tephras. Spikes 2.2, 2.3, and 2.4 may correlate with the Towada tephra series (seven correlative candidates), spike G3.1 with a tephra derived from Ontake volcano (MIS 5b–5c), and spike G3.2 with Towada-Castera (To-CP) or Towada-Aosuji (To-AP; both MIS 5b–5d).

(2) Visible tephra layers in the VCD correspond well to glass shard spikes, and many of them have been correlated with known tephras. We reclassified a tephra layer previously correlated with To-Of as a sand layer with very few glass shards. Therefore, the VCD sometimes over-records tephra layers.

(3) We interpreted spike G0.1 as reworked material from the underlying spike G0.2 (To-H), and spikes G0.3 and G0.4 as reflecting repeated reworking of the spike G0.5 tephra (To-BP2). Similarly, spikes G0.8 and G0.9 were produced by repeated reworking of the underlying spike G1 (To-Of). We also classified spikes G1.3 and G1.4 as post-depositional mixtures of Spfa-1 shards and shards of other tephras. We interpreted the decreasing-upward glass shard profiles above spikes G3 and G4 as an indicator of immediate reworking of the SK and Toya tephras just after their emplacement.

(4) Ash patches just below the Toya horizon probably reflect gravitational loading but they do not introduce serious uncertainty to the stratigraphic position of

the Toya tephra in the C9001C cores.

(5) Whether a marine tephra is preserved as a tephra layer depends on the depositional and post-depositional processes to which it is subjected, as well as on the eruptive volume and distance from the source. Cryptotephras in marine cores have significant potential to contribute to marine tephrostratigraphy.

Acknowledgements

Samples from the C9001C cores were provided by the Japan Agency for Marine-Earth Science and Technology (JAMSTEC). Secondary standard glasses of the MPI-DING series were provided by S. Brigitte and K.P. Jochum (Max Planck Institut fuer Chemie). We thank A. Furusawa for chemical analyses. We thank N. Hamada (JNES), M. Koshigai, and M. Mukai (Sunco Consultants) for constructive comments. We also thank T. Tomiyama, Y. Ichiyama, and N. Ahagon (JAMSTEC) and S. Tonai (Kochi University) for help in sampling the cores. Review comments by J.-I. Kimura and T. Hasegawa improved the manuscript. Some figures were prepared with Generic Mapping Tools version 4.2.0 (Wessel and Smith, 1998). This paper is an output of the EXTRAS project.

References

- Abbott, P.M., S.M. Davies, W.E.N. Austin, N.J.G. Pearce, and F.D. Hibbert (2011), Identification of cryptotephra horizons in a North East Atlantic marine record spanning Marine Isotope Stages 4 and 5a (~60,000–82,000 ka b2k), *Quat. Int.*, 246, 177–189.
- Allan, A.S.R., J.A. Baker, L. Carter, and R.J. Wysoczanski (2008), Reconstructing the Quaternary evolution of the world's most active silicic volcanic system: insights from an ~1.65 Ma deep ocean tephra record sourced from the Taupo Volcanic Zone, New Zealand, *Quat. Sci. Rev.*, 27, 2341–2360.
- Aoike, K. (Ed.) (2007), CK06-06 D/V Chikyu Shakedown Cruise Offshore Shimokita Laboratory Operation Report, 73pp. with Appendices.
- Aoike, K., H. Nishi, T. Sakamoto, K. Iijima, M. Tsuchiya, A. Taira, S. Kuramoto, H. Masago, and Shimokita Core Research Group (2010), Paleooceanographic history of offshore Shimokita Peninsula for the past 800,000

- years based on primary analyses on cores recovered by D/V CHIKYU during the shakedown cruises, *Kaseki (Palaeontol. Soc. Jpn.)*, 87, 65–81 (in Japanese with English abstract).
- Aoki, K. (2008), Revised age and distribution of ca. 87 ka Aso-4 tephra based on new evidence from the northwest Pacific Ocean, *Quat. Int.*, 178, 100–118.
- Aoki, K. and F. Arai (2000), Late Quaternary tephrostratigraphy of marine core KH 94-3, LM-8 off Sanriku, Japan, *Quat. Res. Jpn.*, 39, 107–120 (in Japanese with English abstract).
- Aoki K. and H. Machida (2006), Major element composition of volcanic glass shards in the late Quaternary widespread tephra in Japan – Distinction of tephra using K₂O-TiO₂ diagrams, *Bull. Geol. Surv. Japan*, 57, 239–258.
- Aoki, K., H. Yamamoto, and M. Yamauchi (2000), Late Quaternary tephrostratigraphy of marine cores collected during “Mirai” MR98-03 and MR99-K04 cruises, *Report of Japan Marine Science and Technology Center*, 41, 49–55 (in Japanese with English abstract).
- Aoki, K., T. Irino, and T. Oba (2008), Late Pleistocene tephrostratigraphy of the sediment core MD01-2421 collected of the Kashima coast, Japan, *Quat. Res. Jpn.*, 47, 391–407 (in Japanese with English abstract).
- Aoki, K., T. Suzuki, T. Kawai, T. Sakamoto, and K. Iijima (2012), Mid-late Pleistocene tephrostratigraphy of C9001C and C9002A/B cores off Shimokita, Tohoku Japan, *Japan Geoscience Union Meeting 2012*, MIS27-P23 (in Japanese with English abstract).
- Brendryen, J., H. Haffidason, and H.P. Sejrup (2010), Norwegian Sea tephrostratigraphy of marine isotope stages 4 and 5: Prospects and problems for tephrochronology in the North Atlantic region, *Quat. Sci. Rev.*, 29, 847–864.
- Buhring, C. and M. Sarnthein (2000), Toba ash layers in the South China Sea: Evidence of contrasting wind directions during eruption ca. 74 ka, *Geology*, 28, 275–278.
- Davies, S.M., S. Wastegård, P.M. Abbott, C. Barbante, M. Bigler, S.J. Johnsen, T.L. Rasmussen, J.P. Steffensen, and A. Svensson (2010), Tracing volcanic events in the NGRIP ice-core and synchronising North Atlantic marine records during the last glacial period, *Earth Planetary Sci. Lett.*, 294, 69–79.
- Domitsu, H., J. Uchida, K. Ogane, N. Dobuchi, T. Sato, M. Ikehara, H. Nishi, S. Hasegawa, and M. Oda (2011), Stratigraphic relationship between the last occurrence of *Neoglobobadrina inglei* and marine isotope stages in the northwest Pacific, D/V *Chikyu* expedition 902, hole C9001C, *Newslett. Stratigr.*, 44, 113–122.
- Griggs, A.J., S.M. Davies, P.M. Abbott, and T.L. Rasmussen, A.P. Palmer (2014), Optimising the use of marine tephrochronology in the North Atlantic: a detailed investigation of the Faroe Marine Ash Zones II, III and IV, *Quat. Sci. Rev.*, 106, 122–139.
- Hasegawa, T., M. Sugaya, M. Okada, N. Mochizuki, S. Fujii, and H. Shibuya (2014), Identification of Pleistocene tephra layers in marine sediment core C9001C, offshore Shimokita Peninsula, NE Japan. *Japan Geoscience Union Meeting 2014*, SGL44-06 (in Japanese with English abstract).
- Hopkins, J.L., M. Millet, C. Timm, C.J.N. Wilson, G.S. Leonard, J.M. Palin, and H. Neil (2015), Tools and techniques for developing tephra stratigraphies in lake cores: A case study from the basaltic Auckland Volcanic Field, New Zealand, *Quat. Sci. Rev.*, 123, 58–75.
- Jochum, K.P. and 52 others (2006), MPI-DING reference glasses for in situ microanalysis: New reference values for element concentrations and isotope ratios, *Geochemistry Geophysics Geosystems*, 7, Q02008, doi:10.1029/2005GC001060.
- Kobayashi, S., Y. Ishii, K. Higuchi, Y. Kaminishi, A. Ibusuki, and K. Aoike (2009), 2006 Drilling completion report Shimokita-west. CDEX Technical report Vol. 6, Center for Deep Earth Exploration, Japan Agency for Marine-Earth Science and Technology, 130 pp.
- Kudo, T. and M. Kobayashi (2013), Radiometric dating of tephra from pre-caldera and caldera-forming stages, Towada volcano, Northeast Japan, *Bull. Geol. Surv. Japan*, 64, 305–311 (in Japanese with English abstract).
- Kuehn, S.C., D.G. Froese, P.A.R. Shane, and INTAV Intercomparison Participants (2011), The INTAV intercomparison of electron-beam microanalysis of glass by tephrochronology laboratories: results and recommendations, *Quat. Int.*, 246, 19–47.
- Lisiecki, L.E., and M.E. Raymo (2005), A Pliocene – Pleistocene stack of 57 globally distributed benthic $\delta^{18}\text{O}$ records, *Paleoceanography*, 20, PA1003, doi:10.1029/2004PA001071.
- Lowe, D.J. (2011), Tephrochronology and its application: A review, *Quat. Geochronol.*, 6, 107–153.
- Lowe, D.J. (2014), Marine tephrochronology: a personal perspective. In: Austin, W.E.N., Abbott, P.M., Davies, S.M., Pearce, N.J.G., Wastegard, S. (Eds.), *Marine tephrochronology*, *Geologic. Soc., London*, 398, 7–19.
- Machida, H. (1996), An occurrence of Kutcharo-Shoro tephra at Shironuka, Hokkaido. Inventory of Quaternary outcrops — tephra in Japan: Japan Association for Quaternary Research 40th Anniversary Special Pub., 24 (in Japanese).
- Machida, H. and F. Arai (2003), Atlas of Tephra in and around Japan, University of Tokyo Press, 336pp. (in Japanese with English abstract).
- Mahony, S.H., R.S.J. Sparks, and N.H. Barnard (2014),

- Quantifying uncertainties in marine volcanic ash layer records from ocean drilling cores, *Marine Geol.*, 357, 218–224.
- Manville, V. and C.J.N. Wilson (2005), Vertical density currents: a review of their potential role in the deposition and interpretation of deep-sea ash layers, *J. Geol. Soc. Lond.*, 161, 947–958.
- Matsu'ura, T., I. Miyagi, and A. Furusawa (2011), Late Quaternary cryptotephra detection and correlation in loess in northeastern Japan using cummingtonite geochemistry, *Quat. Res.*, 75, 624–635.
- Matsu'ura T. and J. Komatsubara (2015), Use of pyroxene and amphibole chemistries to refine late Quaternary tephrostratigraphy of deep-sea sequences (Chikyu C9001C cores) and its significance for marine terrace chronology in NE Japan, *XIX INQUA Congress 2015 abstr.*, S05-P05.
- Matsu'ura, T., A. Furusawa, K. Shimogama, N. Goto, and J. Komatsubara (2014), Late Quaternary tephrostratigraphy and cryptotephrostratigraphy of deep-sea sequences (Chikyu C9001C cores) as tools for marine terrace chronology in NE Japan, *Quat. Geochronol.*, 23, 63–79.
- Matsu'ura, T., J.-I. Kimura, Q. Chang, and J. Komatsubara (2017), Using tephrostratigraphy and cryptotephrostratigraphy to re-evaluate and improve Middle Pleistocene age model for marine sequences in Northeast Japan (Chikyu C9001C), *Quat. Geochronol.*, 40, 129–145.
- Song, S.R., C.H. Chen, M.Y. Lee, T.F. Yang, Y. Iizuka, and K.Y. Wei (2000), Newly discovered eastern dispersal of the youngest Toba Tuff, *Marine Geol.*, 167, 303–312.
- Suzuki, T. (1996), Tephra layers originated from Ontake Volcano at Osakada, Shiojiri. Inventory of Quaternary outcrops — tephtras in Japan: Japan Association for Quaternary Research 40th Anniversary Special Pub., 230 (in Japanese).
- Wessel, P. and W. H. F. Smith (1998), New, improved version of Generic Mapping Tools released, *EOS Trans. AGU*, 79, 579.
- Yamamoto, T., J. Itho, M. Nakagawa, T. Hasegawa, and H. Kishimoto (2010), ¹⁴C ages for the ejecta from Kutcharo and Mashu calderas, eastern Hokkaido, Japan, *Bull. Geol. Surv. Japan*, 61, 161–170 (in Japanese with English abstract).
- Yoshimoto, M., M. Amma-Miyagawa, R. Takahashi, M. Nakagawa, and K. Yoshida (2008), Reevaluation of the pre-1640 A.D. eruptive history of Hokkaido-Komagatake volcano, northern Japan, *J. Geol. Soc. Japan*, 114, 336–347 (in Japanese with English abstract).